Lava flow internal structure found from AMS and textural data: An example in methodology from the Chaîne des Puys, France

Sébastien Loock, Hervé Diot, Benjamin van Wyk de Vries, Patrick Launeau, Olivier Merle, Fabienne Vadeboin, Michael S. Petronis

Lava flow internal structure found from AMS and textural data: An example in methodology from the Chaîne des Puys, France

Sébastien Loock [a,*], Hervé Diot [b], Benjamin Van Wyk de Vries [a], Patrick Launeau [c], Olivier Merle [a], Fabienne Vadeboin [d], Michael S. Petronis [e]

[a] *Laboratoire Magmas et Volcans, UMR 6524, OPGC, Université Blaise Pascal, 5 rue Kessler, 63038 Clermont Ferrand, France*
[b] *Université de la Rochelle, France*
[c] *Université de Nantes, France*
[d] *CEREGE, Aix en Provence, France*
[e] *New Mexico Highlands University, Santa Fe, USA*

Anisotropy of magnetic susceptibility (AMS) data analysis is a convenient method used to investigate strain and flow during lava flow emplacement. In order to make a sound interpretation, the origin of the AMS signal must be verified. Two questions must be answered: 1) what phase, or phases carry the AMS signal and 2) when was the AMS fabric acquired? The verification steps themselves can provide extra data for interpreting lava flow conditions. Here, we present a methodology to answer the two questions in a 6 km-long Chaîne des Puys trachybasaltic lava flow that descended into the future site of Clermont Ferrand (France) 45,000 years ago. Knowledge of lava flow emplacement will be useful specifically to this site, if a reactivation of the volcanic chain occurs. The results are also of more general interest to understand lava flow emplacement dynamics.

Curie Temperature, thin sections (optical, SEM, microprobe analysis) and First Order Reversal Curves (FORCS) indicate that the AMS carriers are multidomain (MD) and pseudosingle-domain (PSD) titanomagnetites. 3-D microlite fabric data compared with AMS-fabric elements shows that the AMS ellipsoid is produced by a late-stage microlite fabric deformation, just before complete immobilisation. With this knowledge, and with field structural observations, a vertical section through the lava flow is analysed. Two AMS parameters: magnetic lineation (k_{max}), and degree of anisotropy (A) are significant. The k_{max} displays opposing plunge directions, suggesting reversing simple shear sense. Some k_{max} plunge reversals coincide with degree of anisotropy breaks, also indicating the existence of texturally distinct units. Also, k_{max} plunges can be greater than 45°indicating a vertical pure shear component consistent with inflation. Degree of anisotropy breaks and k_{max} changes correlate with variations in vesicle and/or phenocryst concentrations, underlining that the distinct layers could have been rheologically different. Based on these observations, we propose a qualitative late-stage velocity profile for the flow that requires several distinct layers.

We propose that the flow was layered into distinct rheology units, linked to pre-eruption or in-flow variability. This suggests that during the late stage of emplacement, the flow was subdivided into at least 5 distinct compartments, and each had a different flow history and different behaviour.

1. Introduction

Lava flows are complex liquid–solid flows with strong viscosity variations that cause complex emplacement scenarios (e.g. Self et al., 1998; Hon et al., 2003). Most studies consider lava flows as being relatively homogeneous during emplacement. Here, we look at the flow complexities in a valley-channelled lava flow near its front. The main tool used in this study is the anisotropy of magnetic susceptibility (AMS) technique, supported by detailed mapping and structural analysis.

1.1. AMS definition

Magnetic susceptibility is simply the proportionality constant between the applied and induced magnetic field in a substance. The total susceptibility reflects the contribution of all phases within the material, i.e., ferromagnetic (s.l.), paramagnetic, and diamagnetic mineral phases. Theoretically, as long as the applied field is low, a linear relationship exists between H and M. The induced magnetization and the external magnetic field are linearly related, and so

* Corresponding author.
E-mail address: Loock@opgc.univ-bpclermont.fr (S. Loock).

magnetic susceptibility can be defined by the ratio M/H. Both M and H are expressed in the same units (A/m in the SI) and so magnetic susceptibility is a dimensionless quantity.

Ferromagnets and paramagnets align to the direction of the applied magnetic field (H), while diamagnets align opposite to H. Anisotropy of magnetic susceptibility results from the volume distribution of ALL the magnetic phases within the material (e.g., diamagnetic, quartz; paramagnetic, Fe–Mg silicates; ferromagnetic, Fe–Ti oxides). Thus, the alignment of the atomic moments of ALL phases within the sample (e.g., magnetite, shape anisotropy dominates while hematite crystalline anisotropy dominates), while volume percent of the various phases controls the magnitude of the bulk susceptibility (Tarling and Hrouda, 1993).

An anisotropy of magnetic susceptibility (AMS) measurement of one rock specimen results in an ellipsoid of magnetic susceptibility (k) defined by the length and orientation of its three principal axes, $k_{max} > k_{int} > k_{min}$, which are the three eigenvectors of the susceptibility tensor (Tarling and Hrouda, 1993). The long axis of the magnetic susceptibility ellipsoid k_{max} defines the magnetic lineation, while the short axis, k_{min}, defines the normal to the plane of the magnetic foliation.

1.2. Precautions in using AMS

The AMS tensor is easily obtained and is linked through foliation to the emplacement history of all types of rock (e.g. Tarling and Hrouda, 1993). As noted by several authors (e.g. Borradaile, 1991; Rochette et al., 1992; Borradaile and Henry, 1997; Rochette et al., 1999), several precautionary steps should be taken when verifying the AMS-fabric crystal fabric link and the origin of AMS. These steps can be divided into two groups based on the questions: what mineral(s) carry the AMS and how/when is the AMS fabric developed? Once answered, the AMS can be confidently used as a petrofabric tool and, combined with other textural and structural data, can provide evidence of deformation during emplacement. In addition, the steps used to answer the questions can themselves yield information about the lava flow conditions.

2. Geological setting

We present AMS data from a lava flow from the Chaîne des Puys, France, as part of a project to assess the possible impact of past and future volcanism on the region. The area around the city of Clermont Ferrand has been affected by lava flow repeatedly in the Quaternary, as well as receiving tephra falls from the Chaîne de Puys. The town is sited on a maar and volcanic neck (ca. 150,000 years ago). At about 70,000 years ago, there was a major lava flow influx from the Gravenoire volcano (Goër de Herve et al., 1993; Boivin et al., 2004). At 45,000 years ago, four trachybasaltic lavas flowed down the Tiretaine valley to the city outskirts (Boivin et al., 2004). At about 8000 years ago, trachy-andesitic flows descended to the north side of Clermont Ferrand from the Pariou volcano (Boivin et al., 2004) (Fig. 1).

The Tiretaine lava flows are four superimposed lavas (F1, F2, F3 and F4) that have been canalised into the narrow valley. The lowest lava flow in the section (called F1) is the longest and the highest flow (called F4) is the shortest. These flows have similar trachybasaltic compositions (Boivin et al., 2004). F1, F2 and F4 came from the Petit Puy de Dôme or the Travertin cone whereas F3 came from the Puy de Lacroix (Fig. 1).

The main outcrop studied is located close to the end of the F2 lava, which is 6 km long (Figs. 1 and 2a). The sampled flow outcrops as a 5 m thick cross-section with sampling sites established above and below a street in Royat (Fig. 2b). The top of the flow is preserved. The base is not exposed, but is very close to the outcrop base, as only 10 m away it is seen in the Grotte de Laveuses (Fig. 3b and e). The base of the flow that outcrops in the cave is a platy basal layer about 1 m thick (Fig. 3d). This platy layer is observed low in the study outcrop. Thus, the outcrop provides a near complete vertical section through the flow for study.

From mapping, the lava flow has a general westward flow direction, which is confirmed by grooves orientated 065, 18° towards the East, located under a vesiculated roof (Fig. 3a). The lava flow is close to a pahoehoe, as indicated by the presence of vertical vesiculated pipes (Fig. 3c), vesicle zonation, the limited occurrence of clinker at the base and top (Fig. 3b), and the presence of lateral lobes (Fig. 2b).

In total, twenty-two samples (cylinder cores of 2.5 cm in diameter and > 10 cm long) were collected using a portable gasoline-powered drill with each core orientated using both a solar and magnetic compass.

3. AMS–crystalline fabric relationship method

3.1. AMS carrier determination

The first step in interpreting the nature of the AMS fabric is by fully documenting the magnetic mineral phases within the samples. Curie

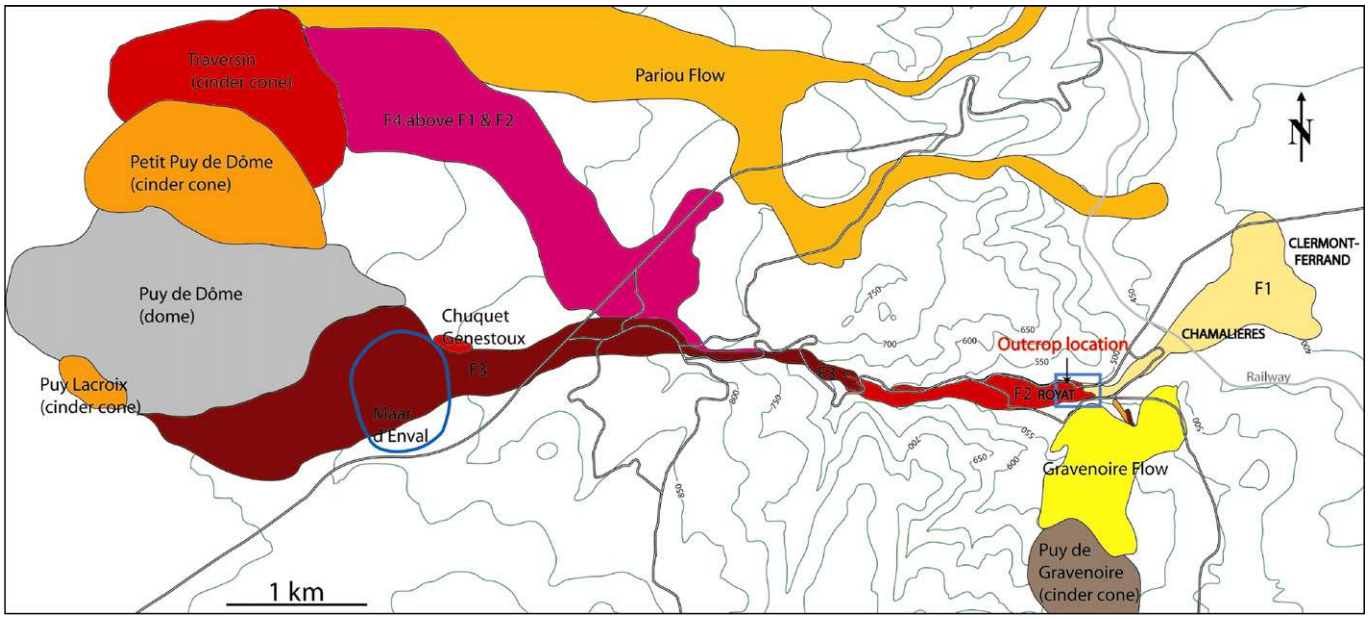

Fig. 1. Map showing the Tiretaine lava flows (F1 to F4) and surrounding lavas, the outcrop location in F2 is indicated by a black arrow. The square shows the close-up map in Fig. 2a.

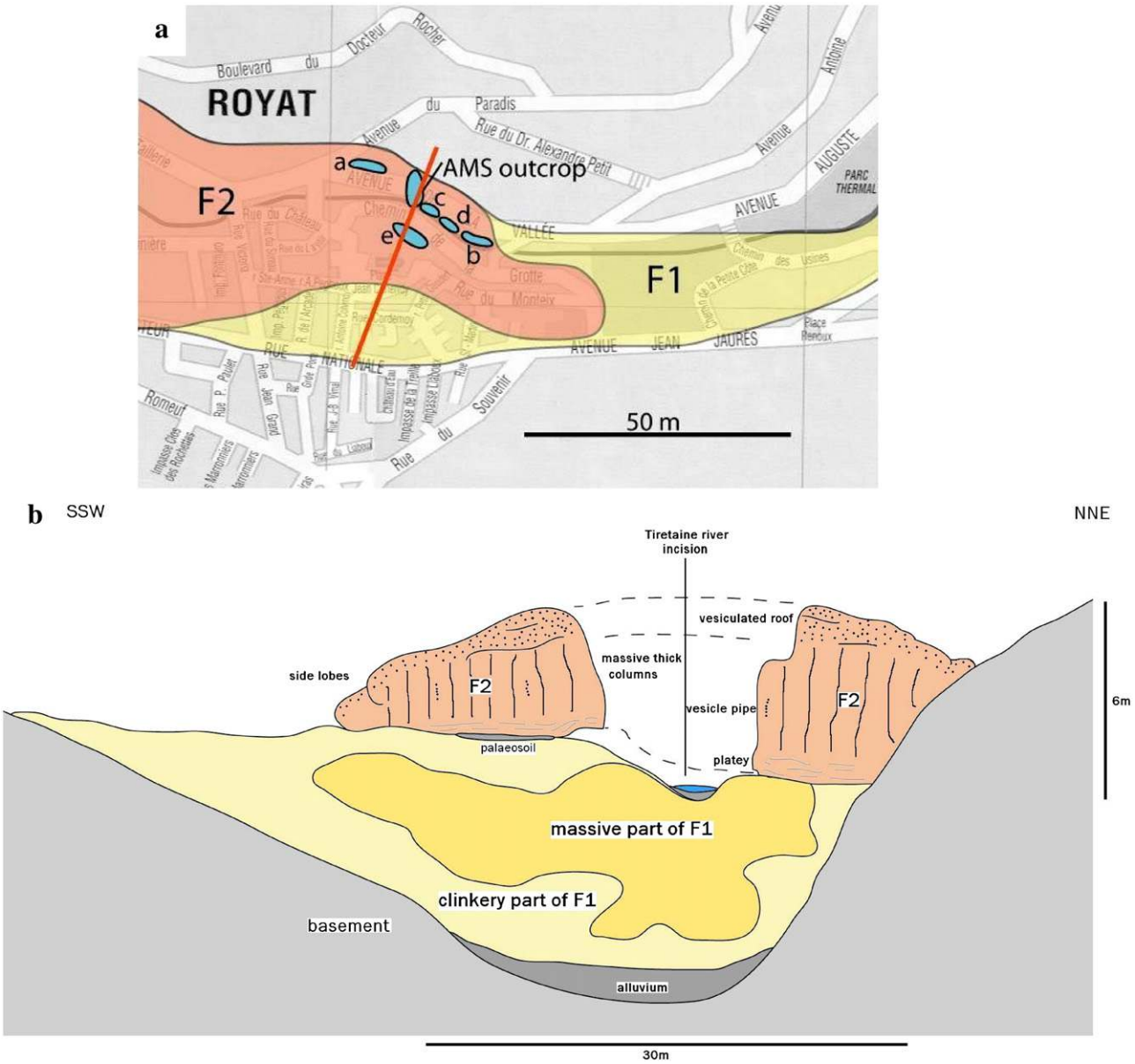

Fig. 2. a. Detailed map showing the studied F2 Tiretaine flow with the main outcrop sampled for AMS and others (a to e) used for textural and structure analysis. Description of these outcrops is provided in Fig. 3. The red bar represents the cross-section profile of b. b. Cross-section (shown in a) displaying the lava flows F1 and F2, and summarizing structural observations on F2. (For interpretation of the references to colour in this figure legend, the reader is referred to the web version of this article.)

Temperature estimates provide a useful indicator of the magnetic phase or phases present within the rock (e.g. Cañón-Tapia, 2004; Hrouda et al., 2005; Bascou et al., 2005). Thin sections are also required to verify the main AMS carrier, define its shape, aspect ratio, concentration and the relationship with the other minerals. Chemical analyses of the main AMS carriers are done to check agreement with the Curie Temperature. Finally, establishing the domain state of the magnetic carrier provides important constraints on the reliability of the AMS fabric as a flow indicator, since SD-magnetite (single domain) have a reversed magnetic fabric, where k_{min} is parallel to the fabric and k_{max} perpendicular, while in MD (multidomain) grains k_{max} lies within the fabric (Rochette et al., 1992; Rochette et al., 1999; Bascou et al., 2005; DeFrates et al., 2006).

3.2. AMS fabric–crystal fabric relationship determination

Once the main AMS carriers are known, the next step is to find out when and how the AMS fabric was acquired. Thin section examination and interpretation of shape preferred orientation (SPO) of each mineral phase will show when the growth of the AMS minerals occurred with respect to the other phases. In lava flows, during cooling, a well-developed microlite fabric generally forms, and this fabric is best compared with the AMS fabric (e.g. Cañón-Tapia and Castro, 2004; Bascou et al., 2005; Nkono et al., 2006). This confirms the assumption that the silicate template controls the AMS fabric (Hrouda et al., 1971; Hargraves et al., 1991).

4. Identification of the AMS carrier in F2

4.1. Curie Temperature

We carried out two measurements from two different samples of continuous thermomagnetic curves (*K–T* curve) at high temperature using a furnace (CS-3) in an Ar atmosphere coupled to a KLY-4 Kappabridge on cylinder cores from F2. Representative thermomagnetic curves are displayed in Fig. 4a and b.

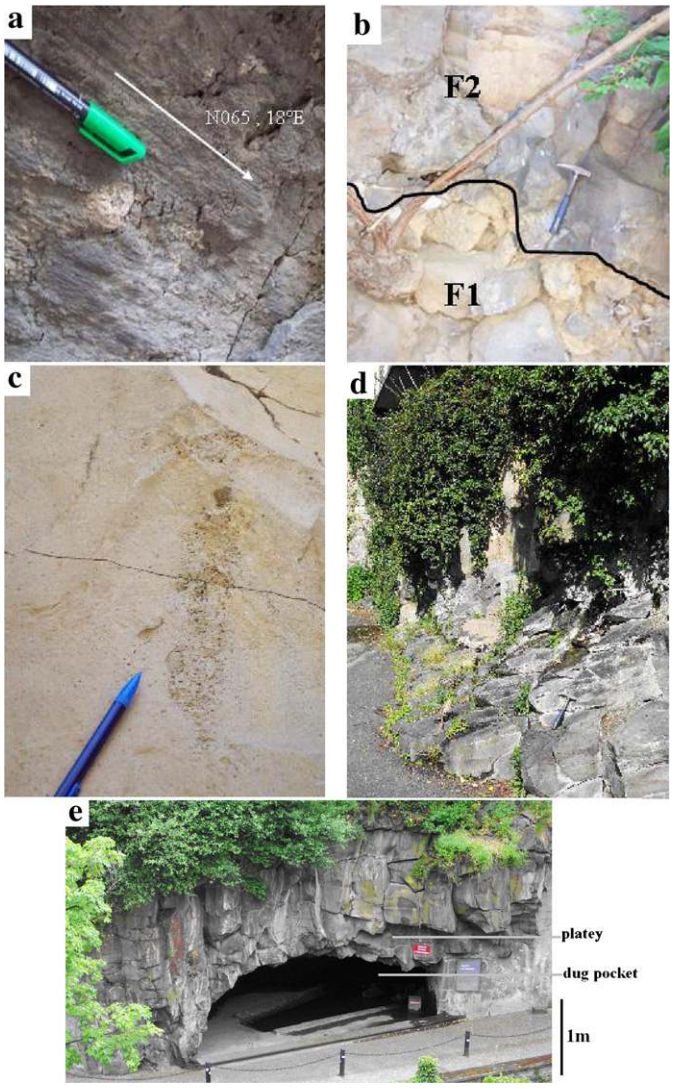

Fig. 3. Outcrops in the vicinity of the main profile, their location is provided in Fig. 2. a: Grooves under a vesiculated roof with a N065,18°E direction. b: Contact displaying the base of F2 with scarce clinker lying over the clinker-rich top of F1. c: A vesicle pipe in F2 indicating a low viscosity interior flow typical of pahoehoe (e.g. Self et al., 1998). d: The platy zone of F2 close to its base. e: The base of F2 where an F1-clinker pocket has been dug out. Platy zone can be seen above the cave, which wraps around cave, but becomes horizontal just 1 m above roof.

The thermomagnetic curves are not reversible and are similar to those from Bascou et al. (2005) from the upper and lower parts of the Saint Thibéry lava flow (French Massif Central). A rapid decrease in susceptibility occurs between 90 °C and 120 °C in Fig. 4a and is less constrained in Fig. 4b. These Curie Temperatures indicate that the main Fe–Ti oxide phases are Ti-rich titanomagnetites (Nishitani, 1981; Dunlop and Özdemir, 1997). By considering the conventional expression of titanomagnetite ($Fe_{3-x}Ti_xO_4$) with $0 \le x \le 1$, microprobe analyses of titanomagnetites give $x \approx 0.7$, which is in good agreement with the observed Curie Temperature (O'Relly, 1984). On continued heating, we note an irreversible slight decrease of susceptibility around 460 °C and at 550 °C. The interpretation of this is less evident, but like Bascou et al. (2005), we propose that this could indicate the presence of metastable titanomaghemite corresponding to low-temperature oxidation of titanomagnetite. Nevertheless, the main Fe–Ti oxide phase and, by inference the AMS carrier, is titanomagnetite with $x \approx 0.7$.

4.2. Thin section investigation

The SEM image displayed in Fig. 5a is representative of all the 35 thin sections made in F2. It shows a good contrast between white titanomagnetites and the other matrix components. The image shows that the titanomagnetite population is not homogenous. Crystals are often skeletal with a wide size range (from some microns to 100 μm) and variable aspect ratio (from 1.2 to 2.7). Microprobe analyses performed on the microphenocrysts gave only titanomagnetite, and none of the suspected titanomaghemite was detected.

Since the lava flow is only 45,000 years old, it is unlikely that the flow is significantly altered, nevertheless we have checked the possibility of any later alteration or weathering, which could have biased the preservation of the primary magnetic signature (e.g. Ade-Hall et al., 1971; Krasa and Herrero-Bervera, 2005). First thin section examination on both optical and electronic microprobe have not revealed presence of any alteration halos around the Fe–Ti oxide phases suggesting that if alteration occurred, it is very weak. To check this, a microprobe colour composite has been performed on a thin section (see Fig. 5b and its legend for the channel inputs) to ensure that magnetic elements have not migrated during an hypothetic alteration episode. Fig. 5b reveals that titanomagnetites are chemically homogenous, so that they appear turquoise blue. There is no release of either titanium or iron, and thus no evidence of any fluid modifying the magnetic mineralogy.

4.3. Magnetic state of the AMS carriers

To determine the magnetic state of the AMS carriers we have used First Order Reversal Curves (FORCs) (e.g., Bascou et al. 2005), instead

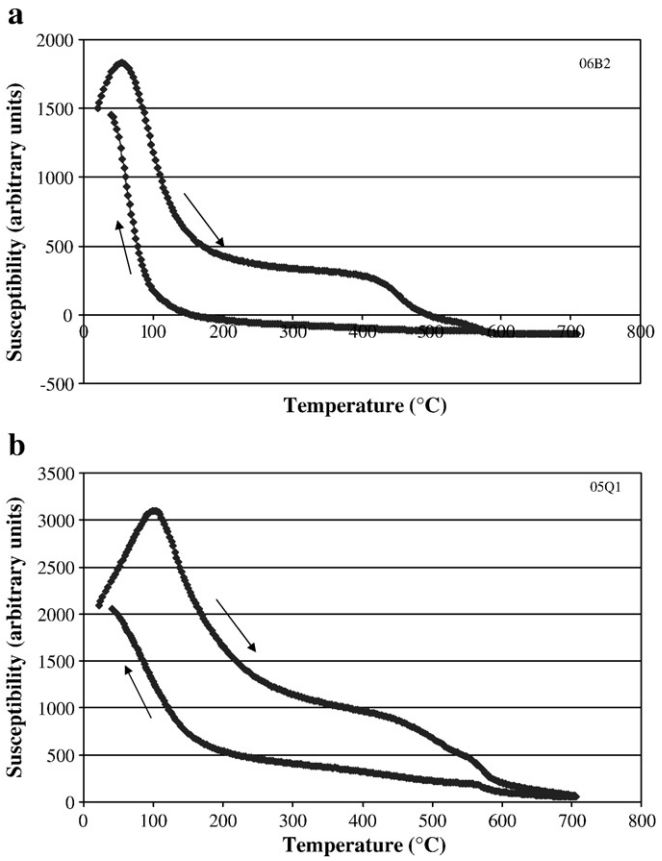

Fig. 4. Representative thermomagnetic curve at high temperature from: a. the B site (sample 06B2) and b. the Q site (sample 05Q1).

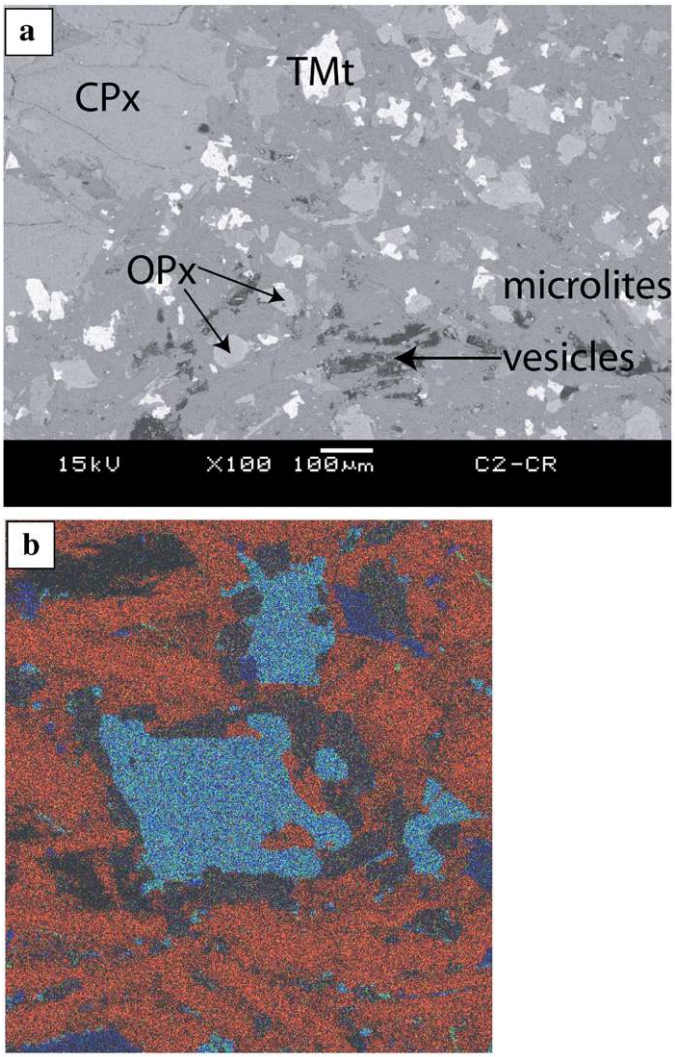

Fig. 5. a. SEM photograph of a sample (C2-CR) from F2. Titanomagnetites (TMt) are white; b. microprobe chemical colour composite of a thin section area (C2-F2; 200×210 µm) from F2: the green channel is for titanium, the blue for iron and the red for aluminium. Thus titanomagnetite appear as turquoise blue (blue+green), while pyroxenes appear as blue and microlites as red. (For interpretation of the references to colour in this figure legend, the reader is referred to the web version of this article.)

of plotting the hysteresis data on a Day plot (Day et al., 1977). A Day plot provides only an average grain size of all the magnetic domain states of the titanomagnetite phases in the sample. This point will be located in a general PSD–SD or MD field and could be the result of a mixed population of different phases. FORCs are expressed by contour plots of a two-dimensional distribution function (Pike et al., 1999; Roberts et al., 2000) and the examination of these contours will reveal the presence of PSD–SD or MD titanomagnetite, even in case of mixing. FORC measurements (100 FORCs per measurement) were performed on six sample location: sites A, C, I, O, Q and U from F2 (see location in Fig. 10a) using the Micro Vibrating Sample Magnetometer of the CEREGE, Institute, Aix en Provence, France. Hb is a measure of magnetostatic interactions while Hc provides indirect information about the magnetic domain structure.

As all six FORC diagrams display similarities in shape, we presented two representative results from sites C and Q (Fig. 6a and b). On diagrams from Fig. 6, contours diverge away from the origin, which was interpreted by Roberts et al. (2000) as a manifestation of MD grains. There is a weak asymmetry of the inner contours around a central peak, indicating a small amount of PSD crystals (e.g. Bascou et al., 2005). The absence of any convergence of the inner contours around a central peak indicates the absence of SD grains. So, in F2, there are mostly MD and some PSD titanomagnetite grains. This is also in agreement with the size range of visible titanomagnetite from 1 to 100 µm in the thin sections. The absence of SD grains (the smallest) is important because, when present, they tend to alter the normal fabric, because of their reverse magnetic contribution (Rochette et al., 1992; Rochette et al., 1999). Thus, the magnetic fabric in F2 can be considered as normal (k_{max} is parallel to the silicate fabric flow direction) and is not weakened by SD grains.

On the six measured FORC-samples, Mr/Ms values range from 0.12 to 0.15 and Hcr/Hc values range from 2.4 to 2.6. Such values in a Day

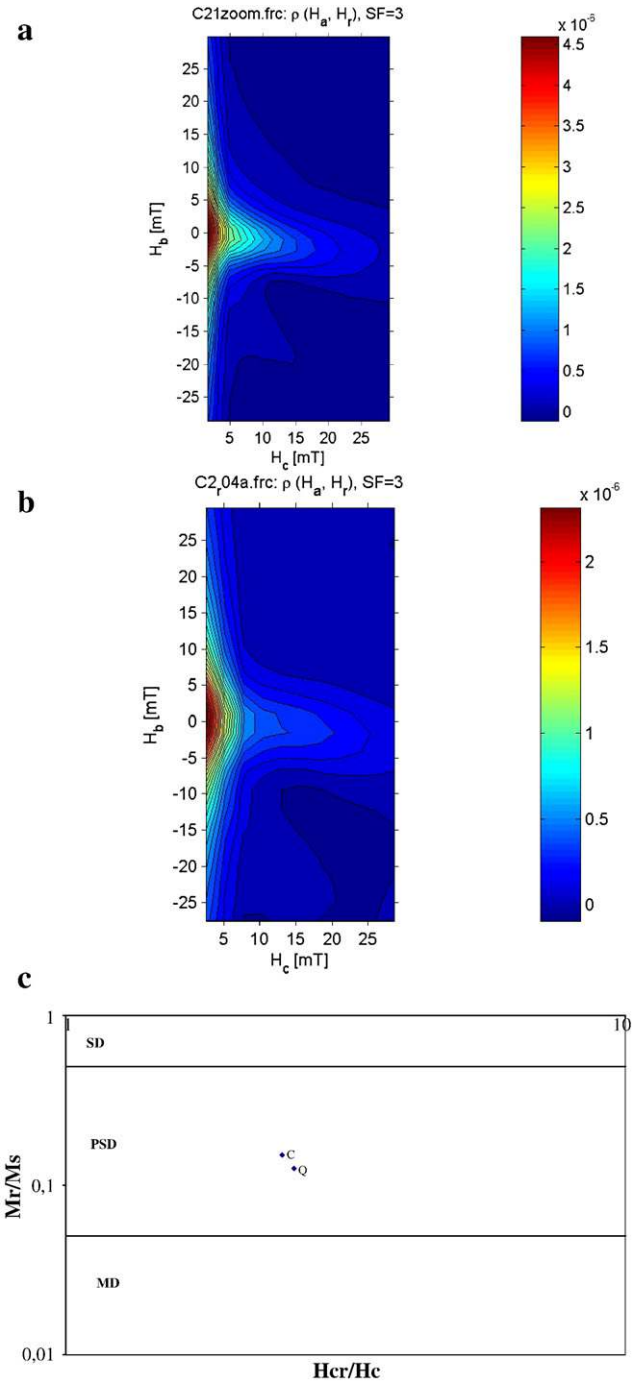

Fig. 6. High resolution FORC diagram in F2 from sample: a. C and b. Q. Smoothing Factor, SF=3. c. Day plot of samples C and Q.

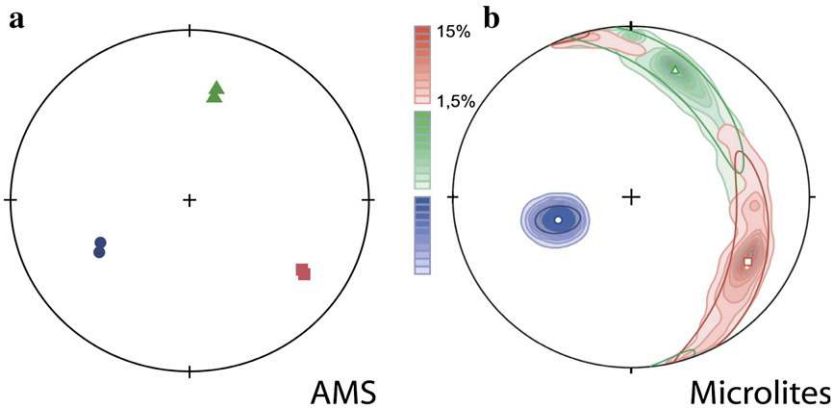

Fig. 7. Equal-area projections (lower hemisphere) of the AMS subfabric (a) and the microlite subfabric (b) at E, in F2. Contours in (b) display the confidence interval. Squares are k_{max}, triangles k_{int} and circles k_{min}.

plot (Day et al., 1977) (Fig. 6c) are plot in the PSD field due to the averaging out produced by the method. The Day plot cannot fully discriminate between all the phases present, while the method described here can. We conclude that the FORC diagrams clearly emphasized the presence of mostly MD and some PSD in the F2 lava flow.

4.4. AMS-fabric conclusions

It has been emphasized that the AMS fabric is carried by a Fe–Ti oxide phase, likely high Ti-magnetite (dominant) and maghemite. In these phases, shape anisotropy of the grains (i.e., aspect ration and relation to the silicate fabric) controls the AMS signal over the crystalline anisotropy of the grains). They display a large size and shape range, so the population is heterogeneous. They are MD and PSD particles, so that there is a normal magnetic fabric signature.

5. The AMS behaviour in F2

The relationship between the silicate fabric (Hargraves et al., 1991) and the AMS tensor was tested by comparing microlite fabric found from image analysis and the AMS fabric. Three thin sections are needed for the image analyses (here vertical North–South, vertical East–West, and horizontal East–West). We have chosen a location in the outcrop where the thin section sample is closest to an AMS sample in order to reduce any lateral variation between the two subfabrics. This location is close to the AMS sample site E (see location in Fig. 10a). While a block sample would have been preferable for this, the outcrop is too massive to allow such sampling. As we had difficulty to isolate some microlites for their neighbours in thin sections, we used the intercept method of Launeau and Robin (1996) (see http://www.sciences.univ-nantes.fr/geol/UMR6112/index.html). This is based on an analysis of the boundary orientation of objects (obtained by filtering and thresholding the digital images obtained using a colour CCD mounted on a binocular, 5× magnification and a rotating polarizer stage microscope of Fuenten (1997), (see http://craton.geol.brocku.ca/faculty/ff/ff1.html). We chose this method rather than the inertia shape tensor method, based on an averaging of orientation and shape parameters of each object, due to the microlite distinction confusion.

The results are displayed in Fig. 7 and Table 1. The main axis orientations of the two tensors (AMS and microlites) coincide. Thus, the two tensors have recorded the same deformation direction. According to Figs. 1 and 2a, the trend of the k_{max} axes are parallel to the lava flow course and thus the tensors reflects in fact the flow direction. This suggests that, in this case (see Section 7.3 for generalization to the 22 samples), the k_{max} axis is the indicator of the flow direction. Given the overall consistency between the AMS and microlite data, we have not considered the imbrication of the magnetic foliation as used in dykes by several authors (e.g., Geoffroy et al., 2002; Callot and Guichet, 2003). The relative elongation of the main axes and, as a consequence, the degree of anisotropy, are not similar and reflects the different shape aspect ratio between titanomagnetites and microlites (see Section 6.2).

Iron–titanium oxides usually crystallize late in basaltic melts at low pressure (e.g. Hill and Roeder, 1974), but here, from thin section observations (Fig. 5) the titanomagnetites have crystallized before the full growth of plagioclase microlites as they display sub-euhedral morphologies. As the tensor axes are similar, we suggest that the flow was active during the growth of microlites. The plagioclases thus control the distribution/orientation of the AMS subfabric.

Finally, with the AMS verification process, we are confident that the AMS results given in Section 7 show the late stage of the flow deformation of F2. This stage is compatible with results from experimental deformation of natural melted lava (Cañón-Tapia and Pinkerton, 2000).

6. AMS parameters and significance of the degree of anisotropy in F2

6.1. AMS parameters

The AMS was measured on 2.2-cm long specimens cut from the orientated cores using the KLY-4 Kappabridge. We used the following parameters:

(1) The mean susceptibility: $km=(k_{max}+k_{int}+k_{min})/3$,
(2) the degree of anisotropy $A=100\,(1-(k_{min}/2k_{max})-(k_{int}/2k_{max}))$
(3) and the shape parameter $T=(2\,(\ln k_{int}-\ln k_{min})/(\ln k_{max}-\ln k_{min}))-1$.

Table 1
Comparison between the AMS and the microlite subfabrics

		k_{max}			k_{int}			k_{min}			Anisotropy
Subfabric	Name	$k_{max\ relative}$	Az_{max}	Inc_{max}	$k_{int\ relative}$	Az_{int}	Inc_{int}	$k_{min\ relative}$	Az_{min}	Inc_{min}	A
AMS subfabric	E	1.014	123.2	25.5	1.000	13.0	36.0	0.986	239.8	43.2	2.130
Microlite subfabric	Em	1.134	120.1	25.3	1.072	18.5	23.1	0.823	251.7	54.6	16.446

If $T<0$ the ellipsoid is linear (prolate) and if $T>0$ it is planar (oblate).

The degree of anisotropy is a parameter quantifying the departure from the isotropic case. As shown by Cañón-Tapia (1994), the different ways to calculate the degree of anisotropy yield qualitatively equivalent results, differing only in their range of numerical values. In this work, we use the A parameter ranging from 0% (isotropic) to 100% ($k_{max} \gg k_{min}$ and k_{int}).

The above formula allows us to have a direct comparison with results from another lava flow where a vertical profile was also performed (Cañón-Tapia and Coe, 2002).

6.2. Significance of the degree of anisotropy in F2

It is generally assumed that the values of degree of magnetic anisotropy are directly linked both to the magnetic mineralogy and the shear strain of the flow (e.g. Hrouda, 1982; Rochette et al., 1992). As we know the likely magnetic phases controlling the AMS, we can discuss the second part of this assumption.

In low concentration suspensions, i.e. without substantial interactions, and for a population of particles with a single aspect ratio, the development of a shape fabric is theoretically cyclic during simple shear. Integration of the equation giving the general motion of a particle (Willis, 1977) yields the critical shear strain γ_T corresponding to one complete rotation of the particle (Fernandez et al., 1983): $\gamma_T = 4\pi/(1-K^2)^{1/2}$ with $K=(n^2-1)/(n^2+1)$ with n = particle aspect ratio. The degree of anisotropy A (the fabric intensity D *in* Ildefonse et al., 1992 and Arbaret and Diot, 1996) reaches a maximum value of $A=n^2$ when the fabric is parallel to the shear direction (Ildefonse et al., 1992). The shear strain at which the maximum intensity is reached is given by $\gamma_C = \gamma_T/4$.

The F2 titanomagnetites display for the visible elements from thin sections variable n from 1.2 to 2.7, and if we consider independently each extreme subpopulation, maximum values of A would be between 1.44 and 7.29%. This explains the low degree of anisotropy values reached on F2 of between 0.9% and 3.0% (see Table 2). Also the γ_C will be between 3.2 and 4.8. We also note here, when considering a microlite fabric with $n=7.5$, that A will reach 56.25%.

If we consider a range of variable aspect ratios and interactions between them, there must be a departure from theoretical curve (Arbaret and Diot, 1996), and a stabilization of the fabric (e.g. Launeau, 2004). Thus, the relationship between the degree of anisotropy and the shear strain is biased. In Fig. 5, we observe that titanomagnetites interact with clinopyroxene pheno- and microphenocrysts, as well as with orthopyroxene microphenocrysts. This indicates that there was an early fabric of mafic phases. Then, as plagioclase microlites appear after titanomagnetite and pyroxene, interactions with this latter phase (see Section 5) will overprint any previous AMS fabric. The fabric finally arrived at is a combination of both, dominated by the plagioclase lath fabric element.

Lastly, we have also to consider, as in most lava flows, a pure shear component (e.g. Merle, 1998) may be present during the stabilization of the magnetic fabric. This may be due to flow thinning or inflation.

7. AMS results and interpretation in F2

Fig. 10a displays the vertical AMS profile on F2 under and above the road. Sample A is the lowest, below which is the very platy near-base of the flow. Sample V is the highest and is taken very near the surface crust of the flow. F2 is vesicle-rich from points R to V in the upper part of the flow and lower down it is massive, with very few isolated vesicles.

7.1. Mean susceptibility k_m

The variation of the bulk susceptibility is displayed in Fig. 9b. The bulk susceptibility ranges from 77.86×10^{-3} SI in P to 31.57×10^{-3} SI in R. Such variations cannot be explained by vesicularity changes, thus we have to consider that the distribution of titanomagnetites cannot be considered as a simple trend as previously observed in other lava flow sections (Cañón-Tapia et al., 1997; Cañón-Tapia and Coe, 2002).

7.2. Shape parameter T

The evolution of the shape parameter (Fig. 10c) displays several switches from the lineation field to the foliation field. These changes are modest as, the ellipsoids have low degree of anisotropy: from 0.915% and 3.023%. Such variations from the lineation to the foliation field were also observed on lava flow sections studied by Cañón-Tapia et al. (1997).

Table 2
AMS measurements and parameters on F2. n is the number of cuttings for each core sample that have been measured

Site, n	k_m	Δk_m	k_{max}				k_{int}				k_{min}				T	ΔT	A	ΔA
	10^{-3}SI	10^{-3} SI	k_{max}	Δk_{max}	Az_{max}	Inc_{max}	k_{int}	Δk_{int}	Az_{int}	Inc_{int}	k_{min}	Δk_{min}	Az_{min}	Inc_{min}			(%)	
A, 2	76.17	0.01	1.020	0.005	69.70	47.0	1.002	0.007	336.2	3.3	0.978	0.002	243.2	43.0	0.176	0.006	2.943	0.056
B, 2	68.52	0.06	1.016	0.003	270.4	27.1	1.001	0.005	2.8	4.9	0.984	0.007	102.4	62.3	0.054	0.002	2.349	0.042
C, 3	72.58	0.02	1.015	0.004	295.9	14.6	1.000	0.004	201.2	16.9	0.985	0.004	64.1	67.4	0.030	0.001	2.134	0.036
D, 3	74.98	0.03	1.014	0.005	289.5	13.6	0.999	0.004	185.9	44.4	0.987	0.004	32.3	42.3	−0.084	0.003	2.052	0.035
E, 3	73.97	0.02	1.014	0.000	123.2	25.5	1.000	0.002	13.0	36.0	0.986	0.001	239.8	43.2	0.018	0.000	2.130	0.008
F, 3	64.86	0.03	1.014	0.003	277.6	13.9	1.003	0.002	153.2	66.4	0.983	0.003	12.4	18.6	0.316	0.007	2.003	0.023
G, 3	65.89	0.01	1.013	0.003	79.7	13.9	1.002	0.002	174.6	18.5	0.985	0.004	314.9	66.5	0.162	0.004	1.970	0.023
H, 6	67.33	0.02	1.014	0.004	99.5	5.4	0.999	0.007	355.2	69.3	0.987	0.006	191.5	19.9	−0.104	0.005	2.071	0.046
I, 3	43.03	0.01	1.015	0.014	89.9	22.5	0.996	0.072	184.6	11.3	0.989	0.069	299.4	64.6	−0.456	0.020	2.217	0.376
J, 3	60.18	0.01	1.016	0.001	88.3	27.6	0.999	0.001	348.6	17.7	0.985	0.002	229.9	56.3	−0.087	0.001	2.392	0.010
K, 2	61.04	0.02	1.016	0.005	139.8	57.2	1.000	0.009	281.7	26.9	0.984	0.004	20.9	17.5	−0.015	0.001	2.352	0.052
L, 2	45.41	0.05	1.009	0.005	334.3	61.2	0.999	0.007	89.0	13.1	0.992	0.007	185.2	25.4	−0.163	0.009	1.344	0.032
M, 3	77.49	0.01	1.006	0.003	255.0	10.8	0.999	0.023	5.1	60.3	0.995	0.022	159.0	27.2	−0.238	0.034	0.915	0.047
N, 2	60.79	0.03	1.010	0.014	81.8	21.3	1.001	0.031	344.8	18.6	0.989	0.023	216.3	62.1	0.146	0.026	1.472	0.119
O, 3	52.02	0.01	1.010	0.003	93.1	50.8	1.000	0.051	335.0	21.4	0.990	0.049	231.0	31.8	−0.025	0.008	1.448	0.155
P, 2	77.86	0.07	1.021	0.001	249.9	36.9	1.005	0.004	149.7	13.2	0.975	0.003	43.4	50.1	0.321	0.007	3.023	0.026
Q, 3	61.79	0.02	1.021	0.005	58.9	31.6	1.000	0.009	187.3	45.3	0.980	0.006	310.0	28.2	0.018	0.001	3.013	0.072
R, 3	31.57	0.01	1.010	0.026	102.0	35.7	1.001	0.069	204.9	18.6	0.990	0.049	317.2	49.0	0.094	0.037	1.420	0.243
S, 2	45.02	0.02	1.010	0.004	88.5	38.4	1.000	0.008	352.0	8.2	0.990	0.004	251.9	50.7	0.015	0.001	1.544	0.032
T, 3	39.27	0.02	1.011	0.004	260.6	16.3	0.999	0.011	165.3	18.5	0.990	0.012	29.5	64.9	−0.167	0.013	1.601	0.049
U, 2	45.70	0.03	1.009	0.003	88.6	16.8	1.002	0.007	356.6	5.7	0.989	0.008	248.0	72.3	0.247	0.013	1.346	0.029
V, 3	56.07	0.02	1.014	0.034	70.3	14.4	1.001	0.034	311.9	61.6	0.985	0.001	167.2	24.1	0.097	0.014	2.117	0.215

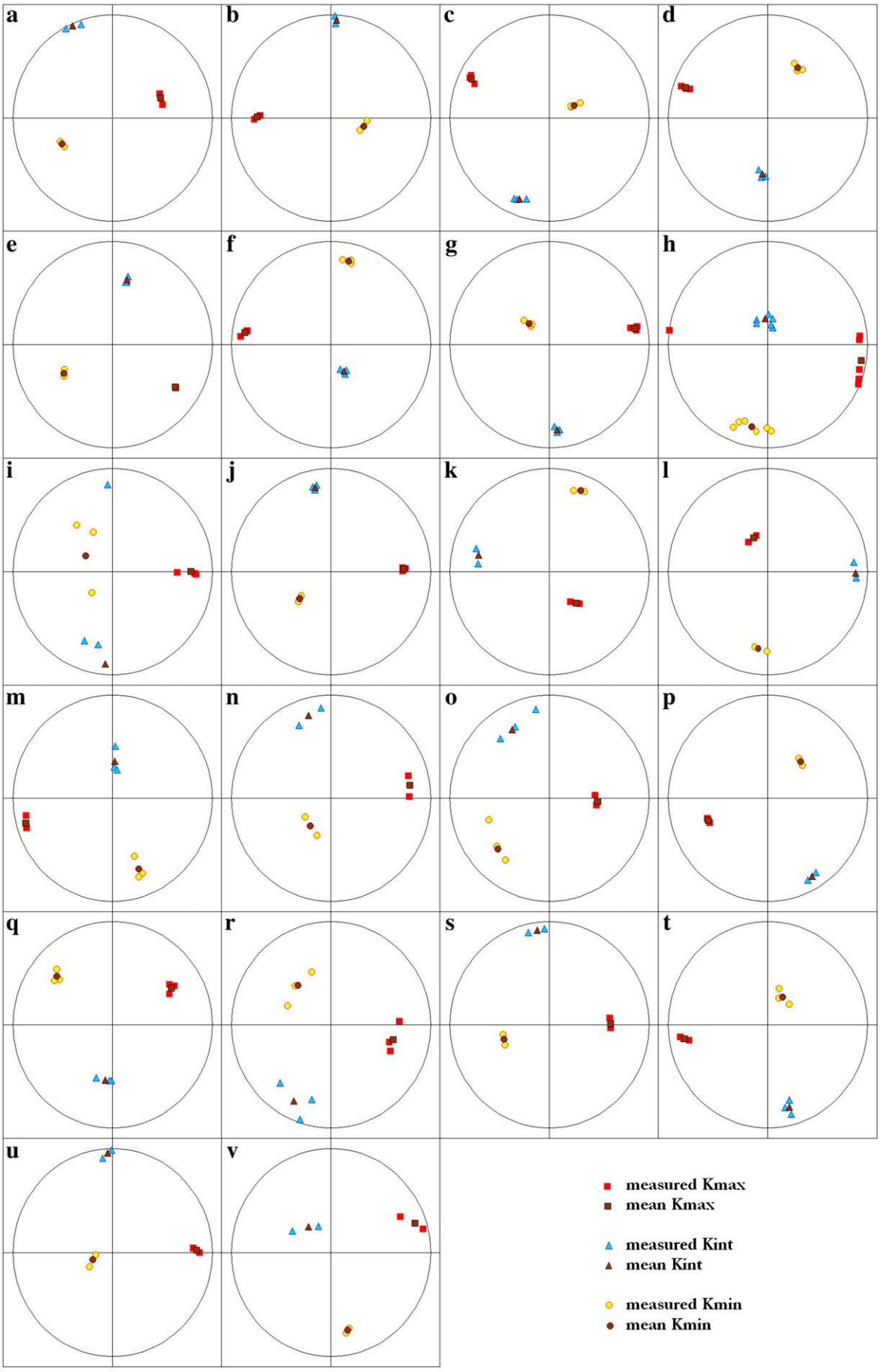

Fig. 8. F2 stereograms of the anisotropy of magnetic susceptibility. Equal-area projection (lower hemisphere).

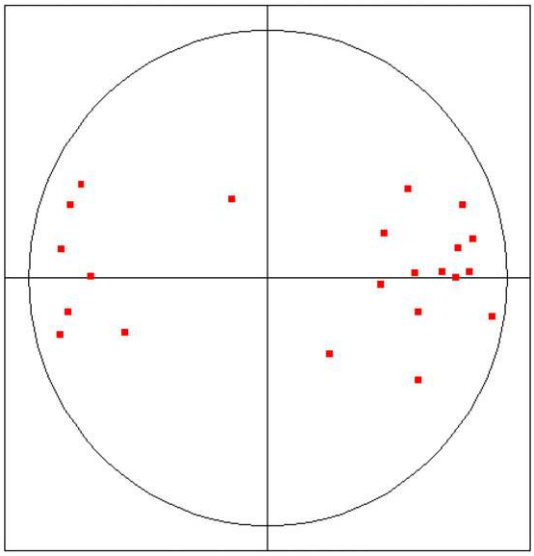

Fig. 9. F2 stereogram of the k_{max} axis on the 22 samples drilled all over the outcrop. Equal-area projection (lower hemisphere).

7.3. Eigenvector orientations and dip

Values of azimuths and inclinations of the eigenvectors (Table 2 and in Figs. 8 and 9) show a relatively good agreement with the westward flow direction of F2 as previously observed in Section 5 (alignment of k_{max} azimuth). Thus, the AMS tensor has recorded the flow deformation over the whole F2 section and again (see Section 5) we consider the k_{max} azimuth as the indicator of the flow direction and not the magnetic foliation used in dykes by several authors (e.g. Geoffroy et al., 2002; Callot and Guichet, 2003).

k_{max} plunge directions (Fig. 10e) switch from eastward to westward and some are steep (over 45°). This is the first time, to our knowledge, that more than one switch of the k_{max} axes has been reported. Single k_{max} axis switches from the upper and the lower flow parts are commonly observed (Bascou et al., 2005). These opposing dips are interpreted as being due to the velocity profile characteristic of a roofed lava (Cañón-Tapia, 1996). During flow cooling, the roof thickness increases and the vertical velocity profile evolves as a function of time. Modelling of strain within lava flows (Merle, 1998, 2000) showed that for a roofed flow or a tunnel, strain evolves toward a central low strain area of highest velocity. Clearly, then, F2 must have a more complicated history.

A first explanation would be a succession of several lava units each undergoing a basal and top shear. According this explanation, we have to suppose that a sample close to the F2 base (under sample A) has to display a westward k_{max} dip direction (Fig. 10e). In this way, the contact between each lava unit will be located where there is a k_{max} dip change from westward (top) to eastward (bottom) that is to say between S&T, O&P, K&L, E&F and A&B.

A second possibility would be an inhomogeneous flow with rheological steps. These variations may be attributed bulk compositional zones in the flow, volatile loss, as well as differential crystallization.

A third possibility is that the lava has occasional upstream flow events.

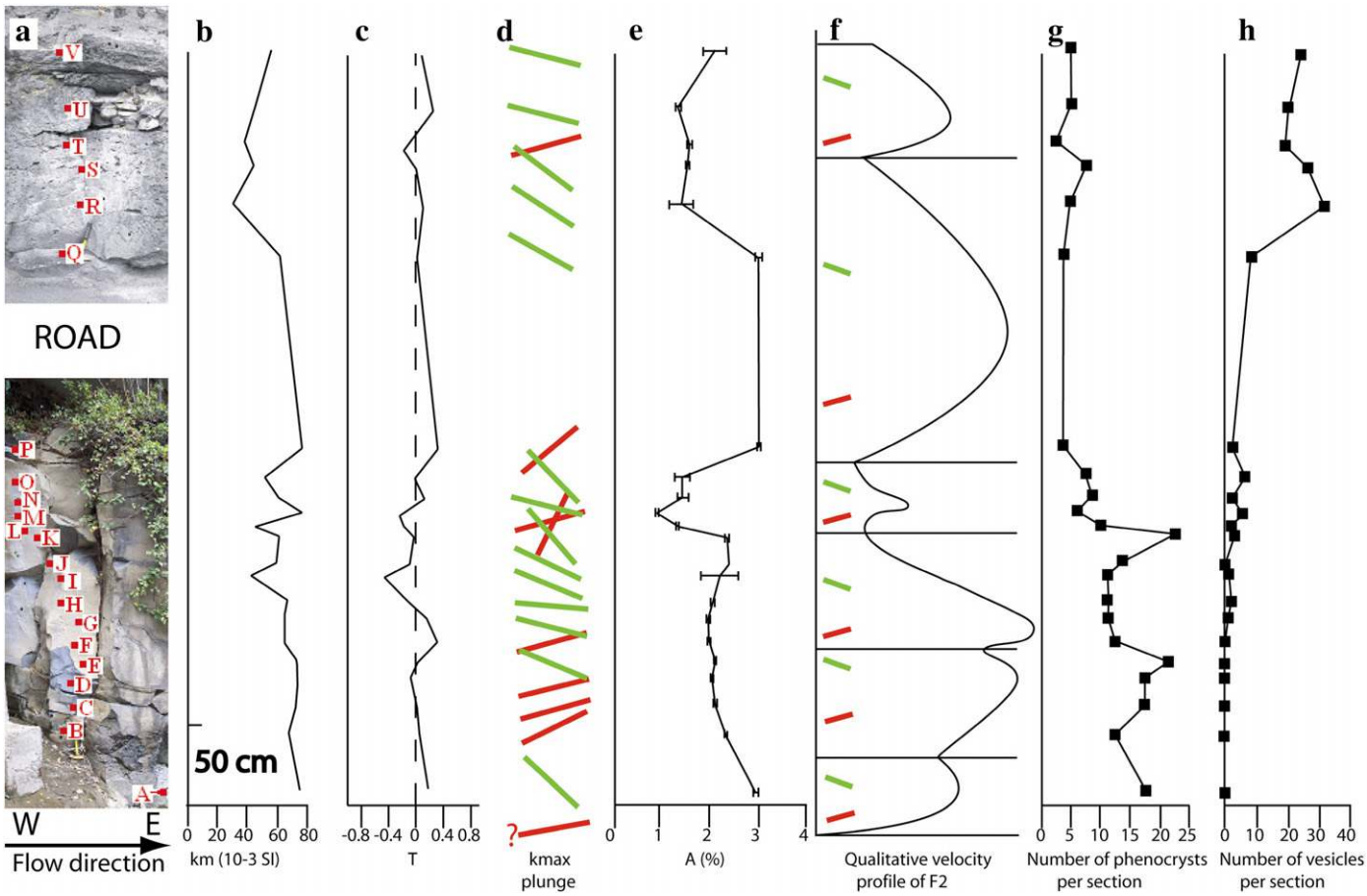

Fig. 10. a. The 5 m-high outcrop on F2 with the core locations — b. Evolution of the mean susceptibility — c. Evolution of the magnetic shape parameter — d. Evolution of the k_{max} dip plunge — e. Evolution of the magnetic degree of anisotropy — f. Qualitative velocity profile deduced from Fig. 9e and f — g. Evolution of the number of phenocrysts per section — h. Evolution of the number of vesicles per section.

Table 3
Evolution of the number of phenocrysts and the number of vesicles per section 2.2 cm in diameter. The evolution of the degree of anisotropy is also provided for direct comparison

Site	Number of phenocrysts per section	Number of vesicles per section	Degree of magnetic anisotropy *A* (%)
A	18	0	2.943
B	14	0	2.349
C	18	0	2.134
D	18	0	2.052
E	21	0	2.130
F	14	0	2.003
G	13	1	1.970
H	13	2	2.071
I	13	1	2.217
J	15	0	2.392
K	22	3	2.352
L	12	2	1.344
M	9	5	0.915
N	11	2	1.472
O	10	6	1.448
P	7	2	3.023
Q	7	8	3.013
R	8	31	1.420
S	10	26	1.544
T	6	19	1.601
U	8	20	1.346
V	8	24	2.117

A fourth possibility is that the flow is wavy, and the vertical profile is recording the progressing lateral set of undulations. We discuss each of these possibilities in Section 7.5.

The inclination of k_{max} can locally be greater than 45°, that is to say greater than the incremental elongation axis dip in simple shear. The largest value is located at L, where the inclination reaches 61.2° (Table 2). Such values can also be found in other flows (e.g. Walker et al., 1999; Cañón-Tapia and Coe, 2002; Cañón-Tapia, 2004) but have not always received any interpretation. Mostly, it has been assumed that lava flows are mainly submitted to simple shear, but k_{max} dips greater than 45° suggest pure shear. Thus, here lava flow emplacement results in a combination of simple shear and pure shear. In our case, the simplest way to obtain k_{max} dips greater than 45° is by vertical pure shear elongation. Such stretching can occur when a lava flowing into a larger valley is entering in a narrower valley or filling a flow front: in both cases it will thicken. The two possibilities are combined for F2, as the Royat valley narrows at the outcrop and as F2 is close to its termination (Fig. 2). The pure shear may have affected the whole flow section to different degrees to combine with the simple shear flow deformation. The simple shear can have different gradients in a single simple lava flow (e.g. Merle, 1998) and thus the lava will appear to have already a zoned AMS pattern. In this way, places where simple shear is relatively low will preserve the pure shear signature i.e. k_{max} values greater than 45°.

7.4. Degree of anisotropy A and interpretation

Values of degree of anisotropy (Table 2, Fig. 10e) are low (*A* varies between 0.915% in M and 3.023 in P) and could be explained by the low aspect ratio of titanomagnetites. The values of the degree of anisotropy tend to increase toward the top and base of F2. At these sites, cooling is most rapid and thus inward-flow cooling propagation may quench textures before the degree of anisotropy has been stabilized by the latter interactions and subfabric overprinting as explained in Section 6.2. Thus, close to the lava edges, the degree of anisotropy may not have been stabilized and displays higher values, as previously noted by Cañón-Tapia and Pinkerton (2000) on experimental lava flows. However, in the central part of F2, the degree of anisotropy has probably been stabilized and thus variations cannot be explained by different shear strains.

Two well-constrained breaks of *A* are located between K and M (2.352 to 0.915% in 12 cm) and between O and P (1.448 to 3.023% in 17 cm). Another break is less evident between Q and R (3.013 to 1.420% in 30 cm) where the distance and the error bars are greater. This less evident break can be simply the result in differential titanomagnetite

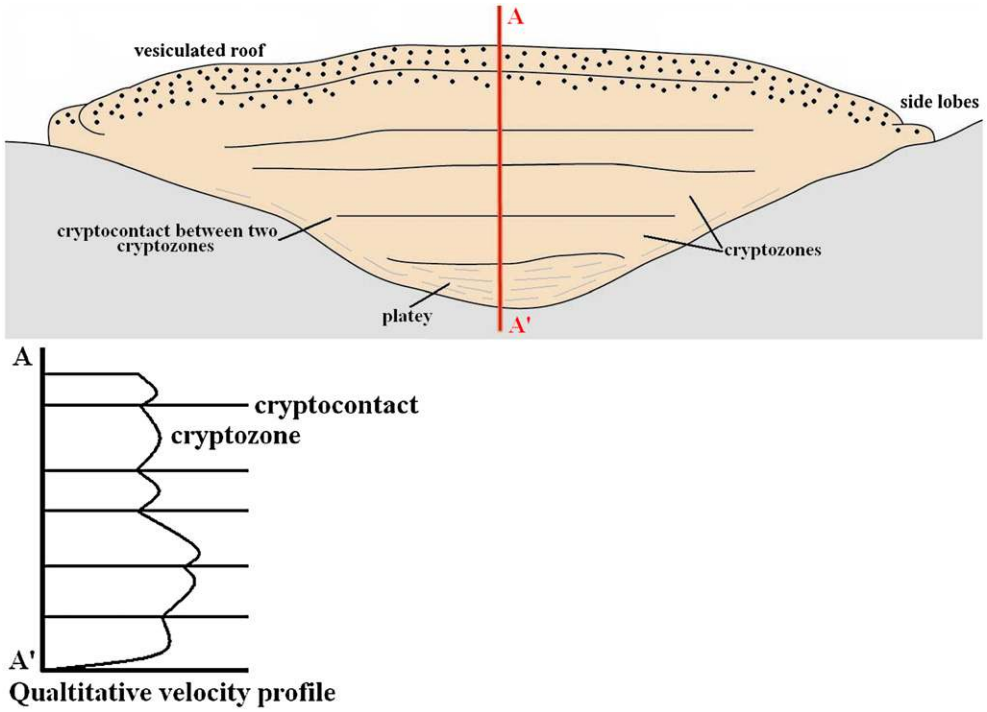

Fig. 11. a. Conceptual section of a lava flow displaying structures found from field, AMS, structural and textural data. AA' represents the vertical section of Fig. 10b — b. Qualitative velocity profile of the same lava flow.

development as it is located at the contact between the vesiculated and non-vesiculated part of F2.

The two well-constrained breaks are both located at k_{max} switches (compare Fig. 10d and e). This indicates that there is a heterogeneity plane located in the lava flow, which could be either a separation between two lava units of the flow or an inhomogeneous flow displaying a rheological threshold due to chemical or crystallization differences.

Whatever the case, each lava flow unit or rheological part displays its own signature and that the passage from one unit to another can be potentially detected by a break in *A* if the signature is sufficiently different.

Leading from the variations of k_{max} plunge directions and the degree of anisotropy, we propose a qualitative velocity profile of F2 during the late stage of deformation (Fig. 10f).

7.5. Rheological insights and interpretation

The possible rheological variations of F2 have been investigated from the evolution of vesicle and mafic phenocryst number density along the same vertical profile as AMS measurements. On each core sample a thin section was made for counting. The counting is thus done on a circular area 2.2 cm in diameter. We are conscious that this method could have large errors, as the studied surface is small, but we consider it is sufficient for finding vesicle and phenocryst *trends* and is also adequate for a direct comparison with AMS parameters (Table 3, Fig. 10g and h). The results are also backed up by direct observation on the outcrop where vesicles and mafic phenocrysts are picked out by the weathering surface.

There is a simple vesicle pattern, with upper vesiculated crust and a massive core (Fig. 10h). The classical lower vesiculated crust of Aubele et al. (1988) is absent here, as we cannot see the F2 base, but it is also not present in other nearby outcrops.

The evolution of the phenocryst number is not so simple. Phenocrysts are more concentrated in the lower part of the flow, indicating probable settling. However, this downward enrichment does not follow a regular trend (Fig. 10g). Direct observations at outcrop show also this heterogeneous pattern. In fact, the downward phenocryst-enrichment is not constant and can display locally an impoverishment. Such a pattern cannot be acquired by simple settlement in a lava flow. We propose that this variation is the combination of an inhomogeneous magma (with phenocryst gradients in the conduit) and the long flow history down a complicated lava channel and tube system.

In Section 7.4, using changes in k_{max} plunge directions and the degree of anisotropy, we located four heterogeneity planes between A&B, K&L, O&P (plunge direction and degree of anisotropy changing), S&T (only plunge direction change) and Q&R (only break of the degree of anisotropy). For each plane we checked for correlations with the vesicle and phenocryst number density variations.

(1) The heterogeneity between Q&R displays no significant variation of phenocrysts, but does for the vesicle numbers: from 31 in Q to 8 in R. Thus this boundary may have a rheologic relationship.
(2) The contact between K&L displays no significant difference in vesicularity, but does in the concentration of phenocrysts: from 22 in K to 12 in L, this indicates a possible rheology difference, if the change is within error.
(3) Vesicularity decreases from 6 in O to 2 in P and the number of phenocrysts for 10 in O to 7 in P. We consider that such variations might be correlated to a rheological change, but are small compared with probable errors.
(4) No vesicles appear in A or in B, but phenocrysts decrease from 18 in A to 14 in B. This difference is so small as to provide no clue to a rheological change.
(5) Between S&T, variations also occur: phenocrysts decrease from 26 to 19 and vesicles from 26 to 19.

Thus, it appears that heterogeneity planes deduced from AMS do in some cases correlate with vesicle and phenocryst number changes that could have a rheological explanation.

In fact, several hypotheses are possible:

1) *Irregular topography: Wavy flow:* The lava flow has been emplaced on very irregular topographic path, which could have led to heterogeneous flow behaviour. Wavy flow patterns may have been produced. However, in the field we have not any proof for this. On the contrary, while the basal platy area of the flow wraps around topographic obstacles, it becomes subparallel over a short vertical distance. In addition, other outcrops do show gas pockets and horizontal fracture levels. This is evidence that wavy behaviour is not present.
2) *Upstream flow:* This is an intriguing possibility. Flow upstream could occur if the lava was thickening at a blocked flow front. A breakout higher on the flow could also create upward drainage. In addition in-flow from the top, for example, could sink and flow back under the main flow. Such flow can be observed in blocked stream channels, but we do not know if it is possible in lava. It is, however, a process worth further consideration. It would indicate that inflation of a flow is more than a static layering up of lava inside the crust.
3) *Multiple inflation episodes:* Another hypothesis could be invoked: the possibility that the lava flow has undergone several inflation or feeding stages. Such an explanation has been invoked by Walker et al. (1999) and Cañón-Tapia and Coe (2002) to explain vertical variations of degree of anisotropy and AMS imbrications in the >45 m- thick Birkett lava flow (Columbia River, USA). In our case, F2 is only 5–6 m thick, allowing us to perform denser sampling. F2 does not display individual vesicular layers as on the Birkett. Some disruptions can be seen in the F2 vesicular zone (Fig. 10a), but they are discontinuous. Vesicularity (Fig. 10i; I think you mean Fig. 10i), and field observations do not display strong breaks in porosity or vesicle concentrations like those in Fig. 3 *in* Walker et al. (1999). So we cannot say that in our case, F2 has undergone several lava pulses, because each pulse would have developed its own vesicular layer. Moreover, Cañón-Tapia and Coe (2002) proposed for the Birkett lava flow that each edge of a new lava input, (i.e. the upper and lower rim subjected to intense shear with the cooled lava) would display a peak in the degree of anisotropy. This is clearly not the case here (see Fig. 10e), where there is a break in the degree of anisotropy but not a peak. Finally, Walker et al. (1999) have pointed out, for the Birkett, that the magnetic fabric in the vesicular part (upper) and the non-vesicular (basal) part have but ONE plunge direction reversal due to ONE symmetric k_{max} plunge direction reversal. In fact, they propose that the level at which injection will occur is always located at the same place, in the middle of the previous still viscous lava, (i.e. in the former no-shear zone separating opposite k_{max} dips). For F2, we have more than ONE reversal, and it would be difficult to imagine that the hypothetical new input of lava could occur randomly in the cooling lava. Thus, from the above observations, we consider that F2 has not been emplaced by a simple inflation model.
4) *Multiple rheological layering:* Due to the variable downward phenocryst-enrichment and the above correlations between AMS breaks and possible rheological variations, we propose that F2 is a heterogeneous flow displaying rheological variations linked to initial variations. It is important to remember that this AMS-evidenced structure is recorded only at a very late stage in the lava flow history. Simply, the AMS ellipsoid records the last incremental motion of flow. The F2 profile is made of at least 5 parts that we interpret as having different rheological conditions. It is possible that if a denser sampling was done, more rheological units might be obtained. F2 is made of several parts and not several stacked flow units, because there is no evidence of contact where break of

degree of anisotropy occurs and there are not several vesicular layers or 'cryptozones'. Such a layered structure could develop by differential flow within the lava along its path, as units with slightly different viscosity flow at different rates, this process could be achieved partly by 'viscous fingering' (Anderson et al., 2005). Fig. 11 summarizes this conceptual point of view according data presented in this paper.

8. Conclusions

In this study, we have illustrated a methodology for the interpretation of lava flow deformation based on soundly constrained AMS and structural/textural observations. The AMS method requires as a first step determination of the main AMS carrier, and a subsequent step to find when the AMS subfabric was acquired. Once these are known, AMS results can be interpreted in the context of other data. We propose that such a procedure should be done every time AMS is used in a new context.

We have applied this methodology to the Tiretaine F2 lava flow from Chaîne des Puys. Firstly, this methodology has allowed us to show that the main AMS carriers are MD and PSD titanomagnetites ($x \approx 0.7$) with irregular size and shape. The absence of SD particles is important, because it means no 'inverse' magnetic fabrics are produced. Secondly, we have demonstrated that the AMS subfabric was acquired during the last stage of deformation of the lava flow. The AMS has a pure shear component and a stabilized simple shear strain component.

We have interpreted each AMS parameter, with a special attention to the k_{max} plunge direction and the degree of anisotropy. Both reversals in k_{max} correlated with breaks in the degree of anisotropy and they indicate the existence of heterogeneity planes separating different lava units. The k_{max} plunge direction greater than 45° indicate a vertical pure shear stretching. From the results we propose a qualitative velocity profile displaying a complex pattern. Uncertainty remains as to the origin of the compartmentalization. Lava waves are discounted due to other evidence. Upslope flow may be possible, but we have no evidence to support it. Multiple punctuated injections, like that proposed for the Birkett flow (Cañón-Tapia and Coe, 2002), are unlikely due to the lack of horizontal vesicle zones.

A layering of several subtly distinct rheological units is our preferred explanation. This interpretation is supported by the vesicle and phenocryst number densities that show subtle correlations with AMS variations. The flow may have individualised such subtle rheological units or 'cryptozones', during magma ascent or during flow the channel and tube system.

Whatever the final explanation for the variations here, the work shows that strain can be variable in a small single flow. Our profile is denser than any yet produced, and further fine-scale investigation may provide even more rheological complexity. The results indicate that lava flows can have very complex internal flow organisation that will lead to complex variations in-flow behaviour. A greater understanding of this will be required if lavas are to be successfully modelled for hazards. In addition, a better understanding will be needed if the use of lava flows as evidence of source conditions and eruption reconstruction is to be successful.

References

Ade-Hall, J.M., Palmer, H.C., Hubbard, T.P., 1971. Magnetic and opaque petrological response of basalts to regional hydrothermal alteration. Geophys. J. R. Astron. Soc. 24, 137–174.

Anderson, S.W., McColley, S., Fink, J.H., Hudson, R., 2005. The development of fluid instabilities and preferred pathways in lava flow interiors: insights from analog experiments and fractal analysis; GSA. Special Paper 396.

Arbaret, L., Diot, H., 1996. Shape fabrics of particles in low concentration suspensions: 2D analogue experiments and application to tiling magma. J. Struct. Geol., vol. 18, 941–950.

Aubele, J.C., Crumpler, L.S., Elston, W.E., 1988. Vesicle zonation and vertical structure of basalt flows. J. Volcanol. Geotherm. Res. 35, 349–374.

Bascou, J., Camps, P., Dautria, J.M., 2005. Magnetic versus crystallographic fabrics in a basaltic lava flow. J. Volcanol. Geotherm. Res. 145, 119–135.

Boivin, P., Besson, J.C., Briot, D., Camus, G., De Goër de Herve, A., Gourgaud, A., Labazuy, Ph., De Larouzière, F.D., Livet, M., Mergoil, J., Miallier, D., Morel, J.M., Vernet, G., Vincent, P.M., 2004. Volcanologie de la Chaîne des Puys, 4ème édition.

Borradaile, G.J., 1991. Correlation of strain with anisotropy of Magnetic susceptibility (AMS). Pure Appl. Geophys. 135, 15–29.

Borradaile, G.J., Henry, B., 1997. Tectonic applications of magnetic susceptibility and its anisotropy. Earth Sci. Rev. 42, 49–93.

Callot, J.P., Guichet, X., 2003. Rock texture and magnetic lineation in dykes: a simple analytical model. Tectonophysics 366, 207–222.

Cañón-Tapia, E., 1994. AMS parameters: guidelines for their rational selection. Pure Appl. Geophys. 142, 365–382.

Cañón-Tapia, E., 1996. Single-grain versus distribution anisotropy: a simple three-dimensional model. Phys. Earth Planet. Inter. 94, 117–131.

Cañón-Tapia, E., 2004. Flow direction and magnetic mineralogy of lava flows from the central parts of the Peninsula of Baja California, Mexico. Bull. Volcanol. 66, 431–442.

Cañón-Tapia, E., Pinkerton, H., 2000. The anisotropy of magnetic susceptibility of lava flows: an experimental approach. J. Volcanol. Geotherm. Res. 98, 219–233.

Cañón-Tapia, E., Coe, R., 2002. Rock magnetic evidence of inflation of a flood basalt lava flow. Bull. Volcanol. 64, 289–302.

Cañón-Tapia, E., Castro, J., 2004. AMS measurements on obsidian from the Inyo Domes, CA: a comparison of magnetic and mineral preferred orientation fabrics. J. Volcanol. Geotherm. Res. 134, 169–182.

Cañón-Tapia, E., Walker, G.P.L., Herrero-Bervera, E., 1997. The internal structure of lavas: insights from AMS measurements II: Hawaiian pahoehoe, toothpaste lava and 'a'ā. J. Volcanol. Geotherm. Res. 76, 19–46.

Day, R., Fuller, M., Schmidt, V.A., 1977. Hysteresis properties of titanomagnetites: grain-size and compositional dependence. Phys. Earth planet. Inter., 13, 260–267.

DeFrates, J., Malone, D.H., Craddock, J.P., 2006. Anisotropy of magnetic susceptibility (AMS) analysis of basalt dikes at Cathedral Cliffs, WY: implications for Heart Mountain faulting. J. Struct. Geol. 28, 9–18.

Dunlop, D.J., Özdemir, Ö., 1997. Rock Magnetism: Fundamentals and Fontiers. Cambridge Univ. Press, Cambridge. 573 pp.

Fernandez, A., Febesse, J.L., Mezure, J.F., 1983. Theoretical and experimental study of fabrics developed by different shaped markers in two-dimensional simple shear. Bull. Soc. Geol. Fr. 7, 319–326.

Fuenten, F., 1997. A computer controlled rotating polarizer stage for the petrographic microscope. Comput. Geosci. 23, 203–208.

Geoffroy, L., Callot, J.P., Aubourg, C., Moreira, M., 2002. Magnetic and plagioclase linear fabric discrepancy in dykes: a new way to define the flow vector using magnetic foliation. Terra Nova, 14, 183–190.

Goër de Herve, A., de Camus, G., Miallier, D., Sanzelle, S., Falguères, C., Faïn, J., Montret, M., Pilleyre, T., 1993. Le puy de Gravenoire et ses coulées dans l'agglomération de Clermont-Ferrand (Massif Central Français): un modèle inhabituel d'avalanche de débris déclenchée par une éruption strombolienne en climat périglaciaire. Bull. Soc. Geol. Fr. 64, 783–793.

Hargraves, R.B., Johnson, D., Chan, C.Y., 1991. Distribution anisotropy: the cause of AMS in igneous rocks? Geophys. Res. Lett. vol 18 (12), 2193–2196.

Hill, R., Roeder, P., 1974. The crystallization of spinel from basaltic liquid as a function of oxygen fugacity. J. Geol. 82, 709–729.

Hon, K., Gansecki, C., Kauahikaua, J., 2003. The transition from aa to pahoehoe crust on flows emplaced during the Pu'u 'O'o-Kupaianaha eruption. US Geological Survey Professional Paper 1676.

Hrouda, F., 1982. Magnetic anisotropy of rocks and its application in geology and geophysics. Geophys. Surv. 5, 37–82.

Hrouda, F., Chlupáčová, M., Rejl, L., 1971. The mimetic fabric of magnetite in some foliated granodiorites, as indicated by magnetic anisotropy. Earth Sci. Planet. Inter. 11, 381–384.

Hrouda, F., Chlupáčová, M., Schulmann, K., Šmíd, J., Závada, P., 2005. On the effect of lava viscosity on the magnetic fabric intensity in alkaline volcanic rocks. Stud. Geophys. Geod. 49, 191–212.

Ildefonse, B., Launeau, P., Bouchez, J.L., Fernandez, A., 1992. Effect of mechanical interactions on the development of shape preferred orientations: a two dimensional experimental approach. J. Struct. Geol. 14, 73–83.

Krasa, D., Herrero-Bervera, E., 2005. Alteration induced changes of magnetic fabric as exemplified by dykes of the Koolau volcanic range. Earth Planet. Sci. Lett. 240, 445–453.

Launeau, P., 2004. Mise en évidence des écoulements magmatiques par analyse d'images 2-D des distributions 3-D d'orientations préférentielles de formes. Bull. Soc. Geol. Fr., 331–350 2004, t. 75, n°4.

Launeau, P., Robin, P.Y.F., 1996. Fabric analysis using the intercept method. Tectonophysics 267, 91–119.

Merle, O., 1998. Internal strain within lava flows from analogue modelling. J. Volcanol. Geotherm. Res. 81, 189–206.

Merle, O., 2000. Numerical modelling of strain lava tubes. Bull. Volcanol. 62, 53–58.

Nishitani, T., 1981. Magnetic properties of titanomagnetites containing spinel ($MgAl_2O_4$). J. Geomagn. Geoelectr. 33 (B12), 171–179.

Nkono, C., Féménias, O., Diot, H., Berza, T., Demaiffe, D., 2006. Flowage differentiation in an andesitic dyke of the Motru Dyke Swarm (Southern Carpatians, Romania) inferred from AMS, CSD and geochemistry. J. Volcanol. Geotherm. Res. 154, 201–221.

O'Relly, W., 1984. Rock and Mineral Magnetism. Blackie, Glasgow. 230 pp.

Pike, C.R., Roberts, A.P., Verosub, K.L., 1999. Characterizing interactions in fine magnetic particle systems using first order reversal curves. J. Appl. Phys. 85, 6660–6667.

Roberts, A.P., Pike, C.R., Verosub, K.L., 2000. First-order reversal curve diagrams: a new tool for characterizing the magnetic properties of natural samples, J. Geophys. Res. 105 (B12), 28461–28475.

Rochette, P., Jackson, M., Aubourg, C., 1992. Rock magnetism and the interpretation of anisotropy of magnetic susceptibility. Rev. Geophys. 30, 209–226 3.
Rochette, P., Aubourg, C., Perrin, M., 1999. Is this magnetic fabric normal? A review and case studies in volcanic formations. Tectonophysics 307, 219–234.
Self, S., Keszthelyi, L., Thordarson, Th., 1998. The importance of pahoehoe. Annu. Rev. Earth Planet. Sci. 26, 81–110 1998.
Tarling, D.H., Hrouda, F., 1993. The Magnetic Anisotropy of Rocks. Chapman and Hall, London. 217 pp.
Walker, G.P.L., Cañón-Tapia, E., Herrero-Bervera, E., 1999. Origin of vesicle layering and double imbrication by endogenous growth in the Birkett basalt flow (Columbia river plateau). J. Volcanol. Geotherm. Res. 88, 15–28.
Willis, D.G., 1977. A kinematic model of preferred orientation. Bull. Geol. Soc. Am., 88, 883–894.